

TiO₂ Hollow Nanofiber/Polyaniline Nanocomposites for Ammonia Detection at Room Temperature

Patrick P. Conti,^[a, b, c] Danilo M. dos Santos,^[a] Irene A. Goldthorpe,^[c] and Daniel S. Correa^{*[a, b]}

Abstract: Ammonia (NH₃) detection has gained considerable attention in agricultural and environmental monitoring, chemical and pharmaceutical processing, and disease diagnosis, which requires the development of sensors with high sensitivity. Herein, we propose a novel gas sensor based on nanocomposites of TiO₂ hollow nanofibers and polyaniline (PANI) for the sensitive detection of ammonia at room temperature. TiO₂ nanostructures in anatase phase were prepared by the combination of coaxial electrospinning and calcination treatment. The resulting material was mixed with PANI and deposited onto gold interdigitated electrodes (IDEs). The hybrid platforms exhibited superior sensing

performance compared to the platform based on their individual phases, which is ascribed to a synergistic effect from p-n heterojunction formation. Specifically, the platforms based on TiO₂/PANI nanocomposite showed a fast response towards NH₃ (e.g., 55 s at 10 ppm) at room temperature (25 °C). Additionally, the platform demonstrated the ability to detect NH₃ at low concentrations (10–30 ppm) and a detection mechanism was proposed to explain the results. Overall, these results show the promise of electrospun TiO₂ hollow nanofibers/PANI composites for the development of high-performance room temperature ammonia sensors.

Introduction

Ammonia (NH₃) is an important volatile that has been widely employed in agricultural and industrial sectors^[1]. However, as NH₃ is also a hazardous pollutant to human health and the environment, it needs to be precisely monitored. For instance, the US National Institute for Occupational Safety and Health has set its recommended exposure limit as 25 ppm (for eight hours) and odor threshold at 5 ppm^[2,3]. In this regard, it becomes important to develop gas sensors for real-time detection of NH₃^[4,5] as well as other gas pollutants in varied environments^[6,7]. Chemiresistive sensors based on semiconductor metal oxides (e.g., ZnO^[8–10], V₂O₅^[11], TiO₂^[12], SnO₂^[13]) have been widely explored for this purpose, owing to their good selectivity, sensitivity and fast response towards ammonia detection.

TiO₂, a typical wide-band n-type semiconductor, exhibits appealing features for NH₃ sensing^[14,15], including low cost, nontoxicity, thermal and chemical stability, and suitable gas-sensing response. Over the past decade, a great variety of TiO₂ nanostructures have been successfully developed and applied towards toxic gas detection^[16]. More recently, electrospun

nanofibers have gained considerable interest to improve the performance of sensors and biosensors due to their high surface-area-to-volume ratio, interconnected porous structure, and low barrier to analyte diffusion^[17]. The versatility of the electrospinning allows the preparation of nanofibers with tailored composition, diameter, and structure^[18]. For instance, core-sheath nanofibers can be prepared by coaxial electrospinning in which two polymeric solutions or melt polymers are injected separately through a concentrically aligned needle^[18,19]. The as-spun core-sheath nanofibers can undergo a further processing step (e.g., calcination, selective dissolution) in order to selectively remove the core and form the hollow fibers. Considering the materials produced by this technique present increased surface area and greater exposure of reactive groups, such strategy has been successfully adopted in the design of ceramic hollow nanofibers^[20] for distinct applications including photocatalysis^[21], solar cells^[22], batteries^[23] and gas sensors^[24].

Although promising, TiO₂-based gas sensors generally require elevated temperatures (200–500 °C) for operation^[25–27]. This represents a great drawback since it implies an energy consumption increase, shortened device lifetime, and limited practical application. To overcome these limitations, metal oxide semiconductors have been combined with conductive polymers (e.g., Polyaniline (PANI), Polypyrrole (Ppy)) and have demonstrated improved sensing performance at room temperature toward different toxic gases^[8,28–30]. Recent works reporting the combination of TiO₂ and PANI in sensing platforms have demonstrated good results for monitoring toxic gases^[31–33]. For example, Yang and collaborators have prepared a chemiresistive platform using nanorods of TiO₂ and PANI for low concentrations of dimethylamine (DMA)^[32]. The authors claimed the good performance presented by the platform was a result of a p-n heterojunction and the distinctive morphology structure, showing that the combination of PANI and TiO₂ can

[a] P. P. Conti, Dr. D. M. dos Santos, Dr. D. S. Correa
Nanotechnology National Laboratory for Agriculture (LNNA)
Embrapa Instrumentação
13560-970, São Carlos, SP (Brazil)
E-mail: daniel.correa@embrapa.br

[b] P. P. Conti, Dr. D. S. Correa
PPGQ, Department of Chemistry,
Center for Exact Sciences and Technology
Federal University of São Carlos (UFSCar)
13565-905 São Carlos, SP (Brazil)

[c] P. P. Conti, Dr. I. A. Goldthorpe
Department of Electrical & Computer Engineering
University of Waterloo
N2L 3G, Waterloo, Ontario (Canada)

be an interesting approach to be explored^[33]. In this context, here we propose a novel composite sensing platform based on electrospun TiO₂ hollow nanofibers and PANI to detect in an easy and fast way NH₃ at different concentrations at room temperature (25 °C). Specifically, electrospun TiO₂ hollow nanofibers in anatase phase were fabricated by combining a coaxial electrospinning process and calcination treatment (Figure 1a). The resulting nanostructures were then functionalized with PANI (Figure 1b) and deposited onto the surface of interdigitated electrodes (IDEs) (Figure 1c). The sensor's performance was examined via impedance spectroscopy measurements (Figure 1d) in the presence of different ammonia concentrations, demonstrating high sensitivity and response for the gas (Figure 1e).

Results and Discussion

Characterization of TiO₂ hollow nanofibers

To determine the phase and crystalline structure of TiO₂ hollow nanofibers, XRD analyses were performed, as shown in Figure 2 (a). It is possible to see diffraction peaks at 25.3° (101), 37.0° (103), 37.8° (004), 38.6° (112), 48.1° (200), 54.0° (105), 55.1° (211), and 62.6° (204) corresponding to anatase phase (JCPDS Card no. 21-1272)^[34]. TiO₂ hollow nanofibers exhibited high

crystallinity as seen by the narrow and sharp XRD peaks. In addition, no other phases were observed, suggesting a material with a high degree of purity. The morphology of TiO₂ hollow nanofibers was evaluated by transmission electron microscopy (TEM), as shown in Figure 2 (b–d). The fibers displayed a double-layer structure, confirming the formation of hollow TiO₂ nanofibers^[35]. Besides, the average diameter of fibers evaluated from distinct TEM images yielded 283 ± 14 nm, corroborating the SEM images discussed next.

TiO₂ nanocomposite characterization

TiO₂ hollow nanofibers, PANI and TiO₂/PANI nanocomposite were analyzed by FTIR as shown in Figure 3 (a). For TiO₂ hollow nanofibers, only one peak at 670 cm⁻¹ was observed, which corresponds to the stretching vibration of the Ti–O bonds^[36]. However, for PANI and the composite several peaks were observed. The broad peak at 3335 cm⁻¹ corresponds to N–H bond stretching, while the two peaks at 1590 and 1496 cm⁻¹ correspond to quinoid and benzenoid ring stretching modes^[37], respectively. The peak at 1375 cm⁻¹ is associated with a stretching vibration of C=N= between the quinoid and benzenoid groups, while at 1050 cm⁻¹ is attributed to in-plane C–H bending vibration^[36]. Therefore, it is possible to notice the vibrational modes of PANI in the composite. However, the

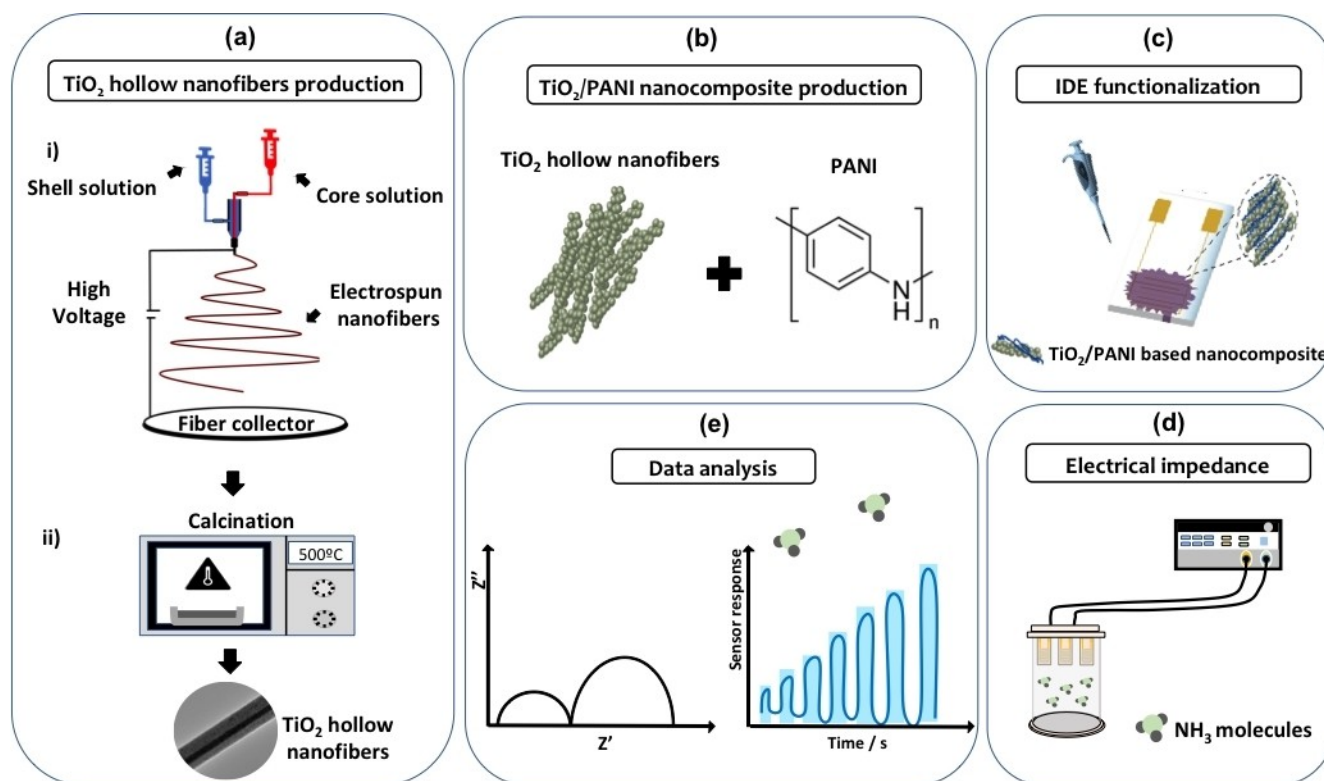


Figure 1. Scheme of nanocomposite-based NH₃ sensor. (a) TiO₂ hollow nanofibers obtention can be divided into two steps: the coaxial electrospinning process (i) followed by calcination at 500 °C (ii), (b) hybrid nanocomposite based on TiO₂ hollow nanofibers and PANI, (c) interdigitated electrodes functionalized by the as-prepared nanocomposite, (d) electrical impedance analysis employing the functionalized electrodes for NH₃ analysis, and (e) NH₃ sensor response using the hybrid platforms.

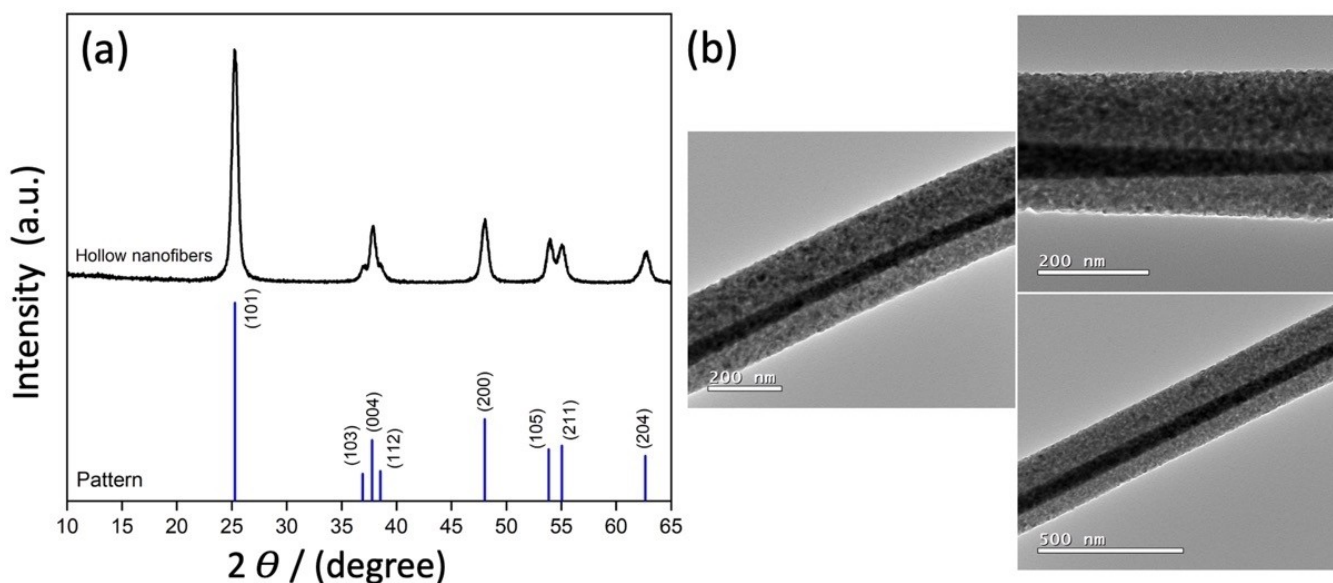


Figure 2. (a) XRD patterns of the hollow nanofibers, confirming crystalline TiO_2 in the anatase phase. (b) Typical TEM images of a TiO_2 hollow nanofiber.

intensity of these bands is lower compared to that of PANI alone. The reason may be the strong interaction of titanium with the nitrogen atoms of PANI, indicating the successful formation of the composite. UV spectroscopy was also used to evaluate the composite gap value (Figure 3b) using Tauc's relation^[38]. The value obtained for TiO_2 hollow nanofibers was 3.20 eV while for the composite was 3.17 eV. The narrowing process observed in the band gap is probably due to the interaction between the materials, indicating in this way a possible better performance as a sensor platform. The micrographs of IDEs modified with TiO_2 /PANI nanocomposites are shown in Figure 4. As can be seen, the IDE surfaces are coated by the nanocomposites. It is possible to observe the dispersion of fibers in a well-connected film, creating two important characteristics: a large amount of material to interact with the gas and good bonding favored by PANI, which facilitates charge transfer. This phenomenon helps the formation (discussed in details later) of a p-n junction^[39]. This dispersion is relevant for the sensing processes explored in this work.

The electrical behaviors of TiO_2 hollow nanofibers, PANI, and TiO_2 /PANI nanocomposites deposited onto IDEs were evaluated by electrical impedance spectroscopy. The Nyquist plots are presented in Figure 5 (a–c). Square points represent the experimental data while the solid lines represent the theoretical fittings using the equivalent electrical circuits shown in Figure 5 (d–f). For platforms based on TiO_2 hollow nanofibers (Figure 5 (a) and 5 (d)), the element R_1 represents the ohmic resistance as a result of the contact between the film and electrode structure, R_2 the inorganic phase resistance, C_1 the double-layer capacitance and QPE1 is a phase constant element used to improve the fitting^[40]. In the case of PANI, the Nyquist plot was fitted with a semi-circle (Figure 5b) and associated with the equivalent electrical circuit as shown in Figure 5 (e)^[41], where R_1 is the intrinsic electrical resistance of the PANI film

combined with the resistance of its interaction with the analyte. R_2 and W are associated with the surface diffusion of charges^[42]. For the TiO_2 nanocomposites (Figure 5 (c) and 5 (f)) the circuit was adjusted by employing the elements used for the ceramic phase and complemented by the presence of the polymer.

The resistivity profile of TiO_2 hollow nanofibers is demonstrated by the high values of $R_1 = 2.8 \times 10^5 \Omega$ and $R_2 = 4.1 \times 10^7 \Omega$, while the conductivity profile of PANI was confirmed by lower resistance values of $R_1 = 118.6 \Omega$ and $R_2 = 1.4 \times 10^3 \Omega$. The nanocomposites exhibited intermediate electrical resistance values between the two isolated phases, namely $R_1 = 310 \Omega$, $R_2 = 4.6 \times 10^4 \Omega$, and $R_3 = 4.9 \times 10^3 \Omega$. Such behavior can be explained by the synergistic effect arising from p-n heterostructure formation between the inorganic and polymeric phases^[43,44]. The use of this hybrid platform is a promising strategy for the development of chemiresistive sensors to overcome the limitations that inorganic oxides present in terms of conductivity at room temperature.

NH_3 sensing performance

The three prepared platforms were analyzed in terms of their responses to different NH_3 concentrations. The data collected at 10 kHz showed the highest resistance response (Eq. 1) across all impedance spectra. This result corroborates with Riul et al.^[45], in which the electrical response at frequencies below 100 Hz is governed by the double-layer effect, whereas frequencies above 100 kHz are ruled by geometric capacitance. In the intermediate frequency range, from 100 Hz to 100 kHz, the response is mainly governed by surface processes related to the material coating the electrode. By comparing the electrical responses towards NH_3 using the three platforms, it can be seen (Figure 6) that the TiO_2 nanocomposite exhibited a

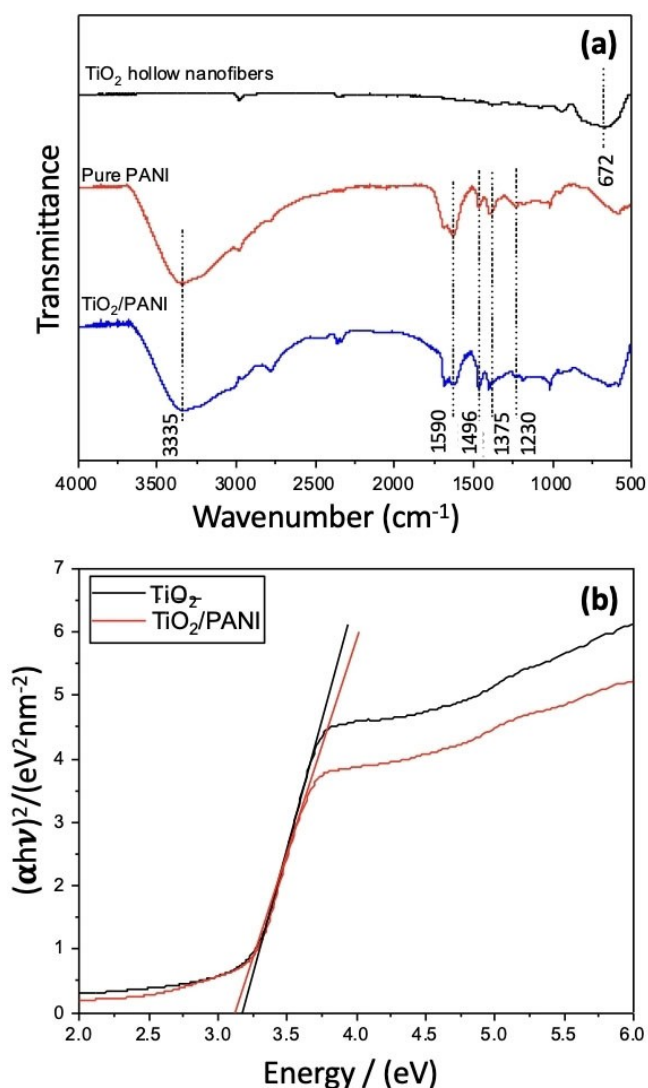


Figure 3. (a) FTIR spectra of: TiO_2 hollow nanofibers, pure PANI and TiO_2 /PANI composite. (b) Tauc's plot for band gap estimation of TiO_2 and TiO_2 /PANI composite.

superior response than its isolated phases (TiO_2 hollow nanofibers and PANI) for all seven selected concentrations (3, 5, 10, 15, 20, 25, and 30 ppm). The greater sensitivity observed for the

hybrid platform is hypothesized to be a consequence of depletion layer formation arising from a synergistic effect between the distinct phases (TiO_2 hollow nanofibers and PANI). Such phenomenon can facilitate electric density percolation within the structure, resulting in a nanocomposite with superior sensing response^[46–48].

Given the better performance presented by the composite-based platform, it was chosen for the next sensing experiments. To evaluate its sensor discrimination capability, three platforms based on TiO_2 /PANI nanocomposites were exposed to five concentrations of ammonia. To perform the analysis, principal component analysis (PCA) was employed, as this technique is capable of reducing data dimensionality while minimizing loss of information^[49]. The PCA plot, obtained with electrical resistance values at 10 kHz for all concentrations employed, is displayed in Figure 7. The data shows great correlation between the triplicate measurements performed for each NH_3 concentration. For concentration values below 10 ppm, the sensor could discriminate the samples with lower accuracy, but on the other hand, for concentrations above 15 ppm, the samples were completely discriminated in PCA plot. Therefore, our results demonstrate the potential of the hybrid platform to be exploited as a sensor for the discrimination of NH_3 (specially for concentrations above 10 ppm) at room temperature.

In order to test the performance of TiO_2 nanocomposite-based sensing platforms, 10, 20, 30, 40, and 50 ppm of ammonia were used. Figure 8 (a) shows the sensor response towards NH_3 exposition at low concentration. An increase in electrical resistance response can be observed for each concentration used. The inset inside the figure shows the platform response when exposed to 10 ppm of NH_3 at room temperature, demonstrating a fast response of 55 s (the time response being defined as the time for the sensor to achieve 90% of resistance maximum value), while the response times for 20, 30, 40 and 50 ppm of NH_3 were determined as 100 s, 48 s, 56 s, 47 s, respectively. These results demonstrate the high sensitivity of the as-developed sensing platform towards NH_3 . The response-concentration relationship for the range 10–50 ppm is presented in Figure 8 (b), yielding a R^2 value of 0.98, thus indicating a good linear dependence. The performance shown by the NH_3 sensing platform here developed is comparable or even superior to similar gas sensors reported in the literature listed in Table 1.

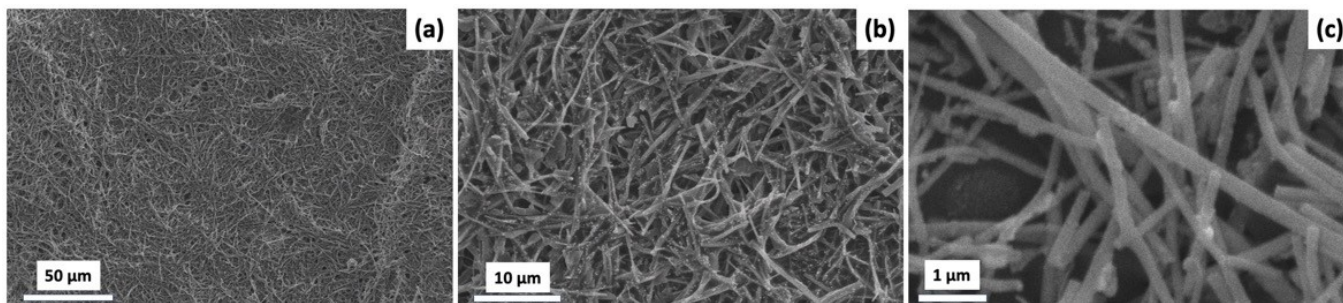


Figure 4. (a) SEM images of TiO_2 /PANI composite deposited onto IDEs. (b) and (c) are magnified images.

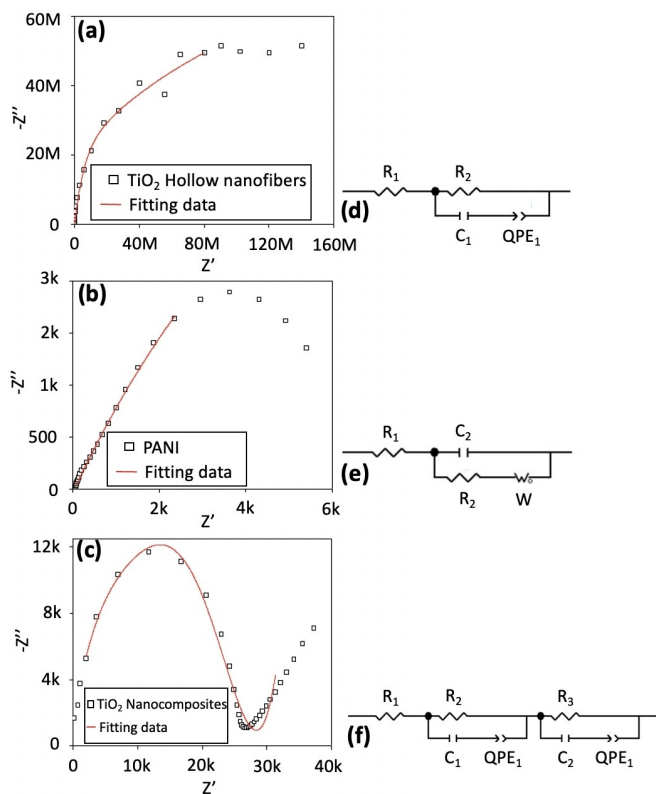


Figure 5. Nyquist diagram for (a) TiO₂ hollow nanofibers, (b) PANI, and (c) TiO₂/PANI nanocomposites. Experimental data are shown by squares, while solid lines represent the fitting using the electrical circuits shown in (d–f).

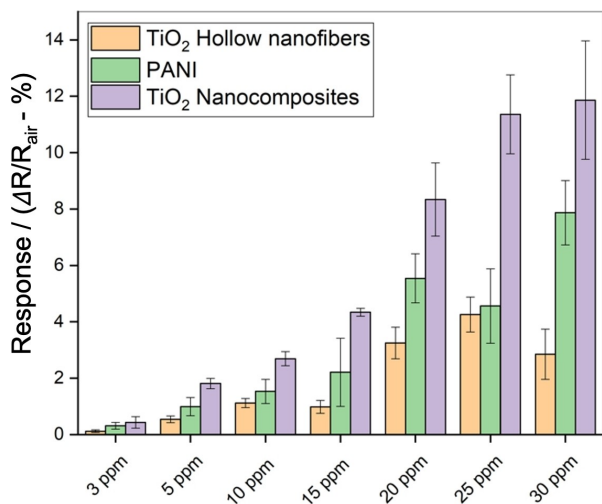


Figure 6. Electrical response of the three sensing platforms to different NH₃ concentrations.

Gas sensing mechanism

TiO₂ is a widely known n-type semiconductor with a band-gap of 3.2 eV, while PANI is a p-type semiconductor with a band-gap of 2.8 eV^[50]. Their mixing generates a hybrid structure that

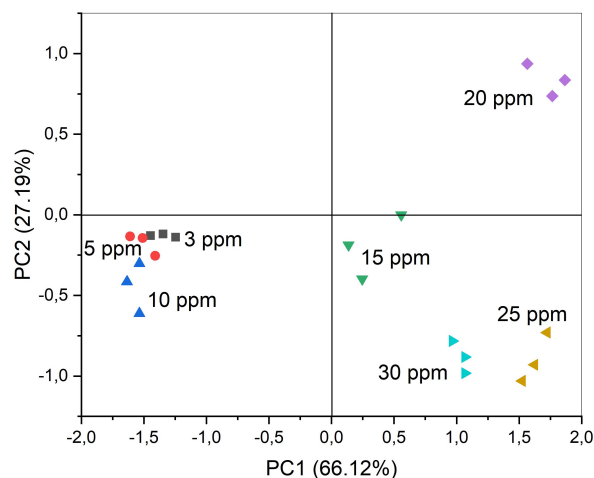


Figure 7. PCA graph for ammonia samples using average electrical resistance values, measured at 10 kHz, based on TiO₂/PANI nanocomposite platforms.

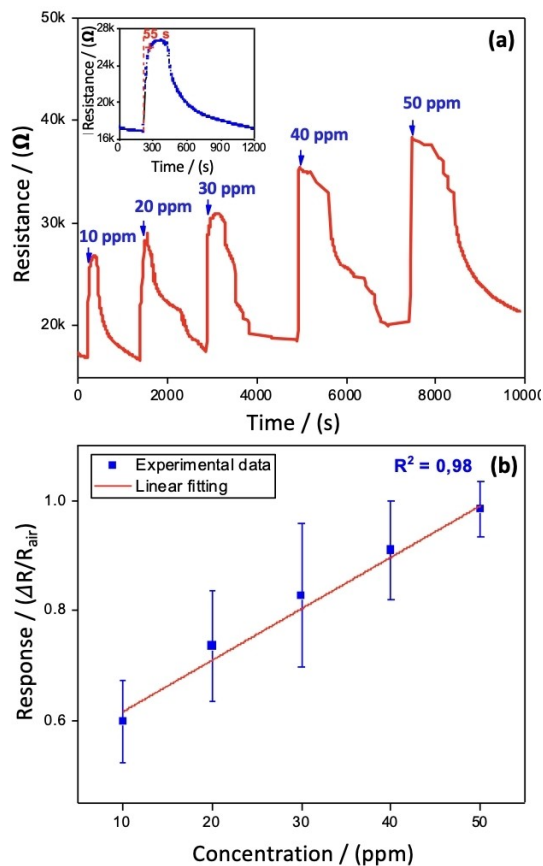


Figure 8. (a) Electrical response of TiO₂/PANI nanocomposite towards different concentrations of ammonia. The inset shows the response time towards 10 ppm of NH₃. (b) Linear dependence of response as a function of NH₃ concentration in the range 10–50 ppm. Gas response evaluated at 10 kHz and room temperature.

presents characteristic of p-n heterojunction, where the creation of an electric field facilitates the charge transfer within the

Sensor material	Temperature/°C	Gas response	Response time/s	Recovery time/s	Limit of detection/ppm	Ref.
TiO ₂ nanoparticles	200	0.12 ^[a,3]	~35 ^[5]	~60 ^[5]	–	[55]
3D SWNT/TiO ₂ nanoparticles	190	0.0597 ^[a,3]	–	–	–	[56]
PANI/SnO ₂ nanoparticles	RT	~0.37 ^[a,1]	12–15 ^[1]	80 ^[1]	–	[57]
Sn-TiO ₂ @rGO/CNT	RT	0.86 ^[a,2]	99 ^[2]	66 ^[2]	–	[58]
PANI/TiO ₂ nanoparticles	RT	~0.35 ^[a,4]	~54 ^[4]	~460 ^[4]	–	[59]
PANI/TiO₂ hollow nanofibers	RT	0.98^[a,4]	47	~750	3	This work

[a] $(R_{\text{gas}} - R_{\text{air}}) / R_{\text{air}}$
Gas response evaluated at: [1] 300 ppm, [2] 250 ppm, [3] 100 ppm, [4] 50 ppm, and [5] 20 ppm

structure, which in turn allows sensor operation at room temperature^[51]. With the adsorption of NH₃ in the structure, the polymer will lose some H⁺, creating vacancies (holes) during the formation of NH₄⁺ (Figure 9 (a))^[52,53]. In this step, the electron recombination process will occur with an increase of charge carriers mainly in the LUMO band of TiO₂ to the LUMO band of PANI (creating electron-hole pairs)^[54], resulting in the observed increase of electrical resistance. This process is illustrated in Figure 9 (b and c), where at the interface of the two phases a depletion layer is formed and a reduction in activation energy as well as NH₃ physisorption enthalpy, are observed^[50,54].

Conclusion

We successfully designed a novel hybrid architecture based on a TiO₂ hollow nanofiber/PANI platform for NH₃ sensing at room temperature. TiO₂ nanostructures were prepared by combining coaxial electrospinning/calcination treatment processes. The

successful formation of hollow nanofibers was confirmed by TEM, while the XRD measurements confirmed the preparation of TiO₂ in the anatase phase. NH₃ sensing performance for the nanocomposite platform at room temperature proved to be superior when compared to those platforms based on the isolated materials. This hybrid platform was exposed to low concentration of NH₃ (10–50 ppm) and showed fast detection response (range of 50–100 seconds) and a sensitivity of 0.98 for 50 ppm of NH₃. Additionally, the platform was capable of discriminating even lower NH₃ concentrations (15–30 ppm), confirmed by PCA analysis. Our results reveal that the TiO₂ hollow nanofiber/PANI nanocomposite is a promising platform for NH₃ sensing at room temperature (25 °C) under 53 ± 5% relative humidity (which performance could also vary under other humidity values), whose architecture could be modified for exploring the monitoring of other volatiles.

Experimental Section

Materials

Poly(vinylpyrrolidone) (PVP, Mw = 10,000 g mol⁻¹), Polyaniline (PANI, Mw = 20,000 g mol⁻¹) and Titanium (IV) butoxide (TNBT, 97% purity) were all purchased from Sigma-Aldrich. Ethanol (99.8%), ammonium hydroxide (NH₄OH), and isopropyl alcohol (99.5%) were obtained from Synth (Brazil). Acetic acid (analytical grade) was obtained from Panreac (Brazil). All the chemical reagents were used without any further purification.

Electrospun TiO₂ hollow fibers preparation

TiO₂ hollow nanofibers were prepared by using coaxial electrospinning. Briefly, the sheath solution was prepared in two steps: i) first, 1.5 mL of TNBT was dissolved in ethanol/acetic acid solution (60/40 (v/v)) upon stirring for 3 h at room temperature; ii) PVP (Cp = 100 mg/mL) was then dissolved in absolute ethanol upon stirring for 3 h at room temperature and added dropwise to the TNBT solution, which was continuously stirred at room temperature for 18 h. Core polymer solution was prepared by dissolving PVP (Cp = 40.6 mg/mL) in ethanol and acetic acid solution (80/20 (v/v)) upon stirring for 3 h at room temperature. The electrospinning process was performed in a homemade setup comprised of a high voltage power supply (Glassman High Voltage, Inc., USA) and two syringe pumps (New Era Pump Systems, Inc., USA). The sheath and core solutions were transferred into 3 mL syringes and pumped separately through the concentrically aligned outer (1.02 mm) and inner (0.65 mm) needles, respectively. The employed electrospinning parameters, optimized in subsidiary experiments (not shown),

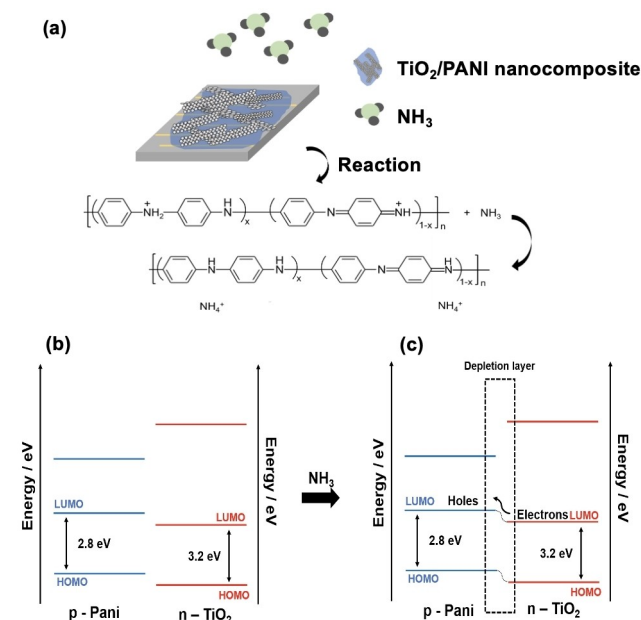


Figure 9. (a) Schematic representation of TiO₂/PANI sensing and reaction mechanism. (b) Energy band diagram in air and (c) in the presence of NH₃.^[37]

were: flow rate of 8 $\mu\text{L}/\text{min}$ and 4 $\mu\text{L}/\text{min}$ for the sheath and core solutions, respectively, working distance = 4 cm, and voltage = 20 kV.

Fibers were directly electrospun onto a stainless-steel drum collector ($L=15.0$ cm, $W=7.3$ cm, and rotation at $\approx 180\text{rpm}$) covered with an aluminum foil for 6 h at $25\pm 2^\circ\text{C}$ and a relative humidity of 25%. Next, the electrospun nanofibers were calcined at 500°C for 4 h in order to create the hollow nanofibers through the selective removal of polymeric matrix and titanium dioxide synthesis. The resulting TiO_2 hollow nanofibers were then stored in a desiccator until further use.

Synthesis of nanocomposites based on TiO_2 hollow nanofibers and PANI

To prepare PANI solution, 3 mg of emeraldine base was dispersed in 3 mL of dimethylacetamide (DMAc) under constant stirring for 12 h. The suspension was filtered through filter paper (80 g/cm^2 and 8 μm pore size, J. Problab). After that, the solution was mixed with HCl excess (1:9 v:v) at $\text{pH}=3$. The TiO_2 nanofiber/PANI nanocomposites was prepared by dispersing 1 mg of TiO_2 nanotubes in 100 μL isopropyl alcohol with the aid of an ultrasonic bath for 1 minute. PANI solution (1 mg/mL) was added in different concentrations (1 to 5% w/v) and the optimized concentration was defined using an optimization process of its electrical resistance values (AC measurements) using a Solartron 1260 impedance analyzer at room temperature (25°C and relative humidity of $53\pm 5\%$). The optimized concentration was found to be 5% of PANI (9% w/v).

Characterization

The morphology of the TiO_2 nanostructure was characterized by transmission electron microscopy (TEM, JEOL JEM2100 LaB6) with an acceleration voltage of 200 kV. To prepare the samples for TEM analysis, the fibers were suspended in absolute ethanol and deposited directly onto 300-mesh carbon-coated Cu grids. The UV-visible absorbance spectra were obtained with a UV-2600 spectrophotometer (Shimadzu) in the range from 185 to 900 nm. Fourier transform infrared (FTIR) spectra were collected using a Bruker Vertex 70 equipment in the $4000\text{--}500\text{ cm}^{-1}$ region. The surface of nanocomposite-modified IDE was investigated with a scanning electron microscope (SEM, JEOL 6510) using an acceleration voltage of 10 kV after sputter coating the samples with gold. The TiO_2 fibers' average diameter was calculated from the SEM images using ImageJ 1.45 software (National Institutes of Health, Bethesda, MD, USA), measuring at least 80 random fibers.

Crystalline structure and phase identification were investigated by X-ray diffraction using a Shimadzu XRD-6000 equipped with $\text{Cu K}\alpha$ radiation ($\lambda = 1.5406 \text{ \AA}$) in the range $10^\circ < 2\theta < 65^\circ$ at a scan rate of $1^\circ/\text{min}$. The operating voltage was 30 kV, and the current was 30 mA.

Electrical characterization of the sensing platforms was performed by AC impedance spectroscopy using a Solartron 1260 impedance analyzer controlled with ZPlot[®]199 software (Scribner Associates Inc.). Parameters employed were: scan rate of 10 pt/dec acquisition, 50 mV and a frequency range from 1 Hz to 1 MHz. The electrodes were connected to the Solartron by an edge connector (2×12 pin, Metaltex) adapted to a glassy chamber sealed with a Teflon lid. Parameters regarding the equivalent electrical circuits were fitted using Nyquist diagram with ZView[®]205 software (Scribner Associates Inc.).

IDE functionalization and sensor measurements

The gold interdigitated electrodes (IDEs) were fabricated by conventional photolithography at the microfabrication laboratory (LMF/LNNano-LNLS, Campinas, SP, Brazil). The IDEs exhibiting 50 pairs of fingers of 4 mm-length, and width and gaps between fingers of 10 μm , were prepared on glass substrates using a layer of chromium followed by gold layer deposition. IDE functionalization was performed by drop casting 3 μL of nanocomposite solution and subsequent drying at room temperature (25°C). NH_3 impedance measurements using the hybrid platforms were carried out at room temperature (25°C) in a home-made cylindrical glass chamber (inner diameter of 70 mm and length of 100 mm). The experiments were performed at a relative humidity of $53\pm 5\%$ (controlled by $[\text{Mg}(\text{NO}_3)_2]$ saturated solution). Two types of electrical measurements were conducted, namely (1) static and (2) gas sensing tests. The static measurements (1) were carried out employing three platforms based on nanocomposites and collected after 30 minutes of system stabilization to ensure complete solvent evaporation and subsequent restoration of the electrical resistance values. The gas concentration was defined by adding specific volumes to obtain 3, 5, 10, 15, 20 and 30 ppm of NH_3 inside the glass chamber. The gas sensing tests (2) were performed with 10, 20, 30, 40, and 50 ppm of NH_3 at 10 kHz at room temperature. With the aid of a syringe, pre-set volumes of ammonia were introduced and a low flow of N_2 was used as a carrier gas. To obtain the resistance variation (ΔR) (Eq.1), the values related to the measurements obtained in the presence of NH_3 (R_{gas}) and without it (R_{air}) were extracted from the real part of impedance, as well as the absolute resistance values obtained at 10 kHz, which were employed to perform the principal component analysis (PCA):

$$\% \Delta R = (R_{\text{gas}} - R_{\text{air}}) / R_{\text{gas}} \times 100 \quad (1)$$

Acknowledgements

The authors thanks the financial support from Fundação de Amparo à Pesquisa do Estado de São Paulo (FAPESP) (grant numbers: 2017/12174-4, 2018/22214-6, 2018/08012-1, and 2019/10885-6), Conselho Nacional de Desenvolvimento Científico e Tecnológico (CNPq), MCTI-SisNano (CNPq/402.287/2013-4), and Rede Agronano-EMBRAPA from Brazil.

Conflict of Interest

The authors declare no conflict of interest.

Data Availability Statement

The data that support the findings of this study are available from the corresponding author upon reasonable request.

Keywords: Ammonia gas sensor · Coaxial electrospinning · chemiresistors sensors · Inorganic/organic composite · TiO_2 hollow nanofibers

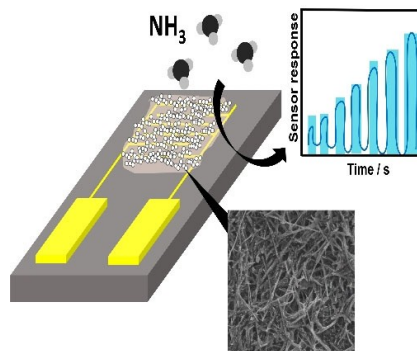
[1] W. A. H. Asman, M. A. Sutton, J. K. Schjørring, *New Phytol.* **1998**, *139*, 27–4.

- [2] R. F. Griffiths, L. C. Megson, *Atmos. Environ. (1967–1989)* **1984**, *18*, 1195–1206.
- [3] J. E. Ryer-Powder, *Plant/Oper. Prog.* **1991**, *10(4)*, 228–232.
- [4] Y. Zhou, Y. Wang, Y. Wang, H. Yu, R. Zhang, J. Li, Z. Zang, X. Li, *ACS Appl. Mater. Interfaces* **2021**, *13*, 56485–56497.
- [5] Y. Wang, Y. Zhou, Y. Wang, R. Zhang, J. Li, X. Li, Z. Zang, *Sens. Actuators B* **2021**, *349*, 130770.
- [6] Y. Zhang, Y. Jiang, Z. Duan, Q. Huang, Y. Wu, B. Liu, Q. Zhao, S. Wang, Z. Yuan, H. Tai, *Sens. Actuators B* **2021**, *344*, 130150.
- [7] Z. Yuan, Q. Zhao, C. Xie, J. Liang, X. Duan, Z. Duan, S. Li, Y. Jiang, H. Tai, *Sens. Actuators B* **2022**, *355*, 131300.
- [8] R. S. Andre, D. Kwak, Q. Dong, W. Zhong, D. S. Correa, L. H. C. Mattoso, Y. Lei, *Sensors* **2018**, *18*, 1058.
- [9] A. Nagar, A. Kumar, U. Tyagi, H. Dhasmana, M. A. M. Khan, S. Husain, A. Verma, V. K. Jain, *Phys. B* **2022**, *626*, 413595.
- [10] S. Kanaparthi, S. Govind Singh, *Mater. Sci. Energy Technol.* **2020**, *3*, 91–96.
- [11] H. Yin, C. Song, Z. Wang, H. Shao, Y. Li, H. Deng, Q. Ma, K. Yu, *Nanomaterials* **2019**, *9*, 317.
- [12] S. S. Rane, D. A. Kajale, S. S. Arbut, S. B. Rane, S. W. Gosavi, *J. Mater. Sci. Mater. Electron.* **2017**, *28(12)*, 9011–9016.
- [13] H. Ren, H. Huo, P. Wang, C. Wang, S. Liu, M. Shen, H. Sun, M. Ruths, *Int. J. Smart Nano Mater.* **2014**, *5(4)*, 257–269.
- [14] W. Meng, L. Dai, W. Meng, H. Zhou, Y. Li, Z. He, L. Wang, *Sens. Actuators B* **2017**, *240*, 962–970.
- [15] Y. Tang, D. Ao, W. Li, X. Zu, S. Li, Y. Q. Fu, *Sens. Actuators B* **2018**, *254*, 1165–1173.
- [16] J. Malallah Rzajj, A. Mohsen Abass, *J. Chem. Rev.* **2020**, *2*, 114–121.
- [17] L. A. Mercante, A. Pavinatto, T. S. Pereira, F. L. Migliorini, D. M. dos Santos, D. S. Correa, *Sens. Actuators Rep.* **2021**, *3*, 100048.
- [18] D. M. dos Santos, D. S. Correa, E. S. Medeiros, J. E. Oliveira, L. H. C. Mattoso, *ACS Appl. Mater. Interfaces* **2020**, *12(41)*, 45673–45701.
- [19] D. M. dos Santos, P. A. M. Chagas, I. S. Leite, N. M. Inada, S. R. de Annunzio, C. R. Fontana, S. P. Campana-Filho, D. S. Correa, *Int. J. Biol. Macromol.* **2020**, *142*, 521–534.
- [20] L. A. Mercante, R. S. Andre, L. H. C. C. Mattoso, D. S. Correa, *ACS Appl. Nano Mater.* **2019**, *2(7)*, 4026–4042.
- [21] W. Chang, F. Xu, X. Mu, L. Ji, G. Ma, J. Nie, *Mater. Res. Bull.* **2013**, *48(7)*, 2661–2668.
- [22] X. Wang, G. He, H. Fong, Z. Zhu, *J. Phys. Chem. C* **2013**, *117(4)*, 1641–1646.
- [23] L. Li, S. Peng, J. K. Y. Lee, D. Ji, M. Srinivasan, S. Ramakrishna, *Nano Energy* **2017**, *39*, 111–139.
- [24] A. Sanger, S. B. Kang, M. H. Jeong, C. U. Kim, J. M. Baik, K. J. Choi, *ACS Appl. Electron. Mater.* **2019**, *1(7)*, 1261–1268.
- [25] P. P. Conti, E. Scopel, E. R. Leite, C. J. Dalmaschio, *J. Mater. Res.* **2020**, *1–9*.
- [26] Z. Li, Z. J. Yao, A. A. Haidry, T. Plecenik, L. J. Xie, L. C. Sun, Q. Fatima, *Int. J. Hydrogen Energy* **2018**, *43*, 21114–21132.
- [27] N. Ramgir, R. Bhusari, N. S. Rawat, S. J. Patil, A. K. Debnath, S. C. Gadkari, K. P. Muthe, *Mater. Sci. Semicond. Process.* **2020**, *106*, 104770.
- [28] P. P. Conti, R. S. Andre, L. A. Mercante, L. Fugikawa-Santos, D. S. Correa, *Sens. Actuators B* **2021**, *344*, 130124.
- [29] J. Gong, Y. Li, Z. Hu, Z. Zhou, Y. Deng, *J. Phys. Chem. C* **2010**, *114*, 9970–9974.
- [30] M. A. Farea, H. Y. Mohammed, S. M. Shirsat, P. W. Sayyad, N. N. Ingle, T. Al-Gahouari, M. M. Mahadik, G. A. Bodkhe, M. D. Shirsat, *Chem. Phys. Lett.* **2021**, *776*, 138703.
- [31] H. Tai, Y. Jiang, G. Xie, J. Yu, X. Chen, *Sens. Actuators B* **2007**, *125(2)*, 644–650.
- [32] M. Yang, X. Zhang, C. Guo, X. Cheng, C. Zhu, Y. Xu, Z. Major, L. Huo, *Sens. Actuators B* **2021**, *342*, 130067.
- [33] D. Nunes, A. Pimentel, A. Goncalves, S. Pereira, R. Branquinho, P. Barquinha, E. Fortunato, R. Martins, *Semicond. Sci. Technol.* **2019**, *34*, 043001.
- [34] W. Li, R. Liang, A. Hu, Z. Huang, Y. N. Zhou, *RSC Adv.* **2014**, *4*, 36959–36966.
- [35] Y. Cheng, W. Huang, Y. Zhang, L. Zhu, Y. Liu, X. Fan, X. Cao, *CrystEngComm* **2010**, *12*, 2256–2260.
- [36] L. Gao, C. Yin, Y. Luo, G. Duan, *Nanomaterials* **2019**, *9*, 493.
- [37] H. Tai, Y. Jiang, G. Xie, J. Yu, X. Chen, Z. Ying, *Sens. Actuators B* **2008**, *129*, 319–326.
- [38] S. K. Sen, T. C. Paul, S. Dutta, M. N. Hossain, M. N. H. Mia, *J. Mater. Sci. Mater. Electron.* **2020**, *31*, 1768–1786.
- [39] Y. Yan, G. Yang, J. L. Xu, M. Zhang, C. C. Kuo, S. D. Wang, *Sci. Technol. Adv. Mater.* **2020**, *21:1*, 769–786.
- [40] F. Lisdat, D. Schäfer, *Anal. Bioanal. Chem.* **2008**, *391*, 1555.
- [41] H. Wang, Y. Zhang, Z. Li, Y. Wu, L. Wu, Z. Jin, *Ionics* **2020**, *26*, 4031–4038.
- [42] C. A. Amarnath, J. Chang, J. Lee, D. Y. Kim, R. S. Mane, S. H. Han, D. Sohn, *Electrochem. Solid-State Lett.* **2008**, *11*, A167.
- [43] Q. Wang, X. Dong, Z. Pang, Y. Du, X. Xia, Q. Wei, F. Huang, *Sensors* **2012**, *12*, 17046–17057.
- [44] K. H. Rahman, A. K. Kar, *J. Environ. Chem. Eng.* **2020**, *8*, 104181.
- [45] A. Riul, A. M. G. Soto, S. V. Mello, S. Bone, D. M. Taylor, L. H. C. Mattoso, *Synth. Met.* **2003**, *132*, 109–116.
- [46] R. S. Andre, R. C. Sanfelice, A. Pavinatto, L. H. C. Mattoso, D. S. Correa, *Mater. Des.* **2018**, *156*, 154–166.
- [47] I. Gawri, R. Ridhi, K. P. Singh, S. K. Tripathi, *Mater. Res. Express* **2018**, *5*, 025303.
- [48] H. Tai, Y. Jiang, G. Xie, J. Yu, M. Zhao, *Int. J. Environ. Anal. Chem.* **2007**, *87(8)*, 539–551.
- [49] I. T. Jolliffe, J. Cadima, *Philos. Trans. R. Soc. London Ser. A* **2016**, *374*, 20150202.
- [50] R. K. Jha, M. Wan, C. Jacob, P. K. Guha, *New J. Chem.* **2018**, *42*, 735–745.
- [51] S. Srivastava, S. Kumar, V. N. Singh, M. Singh, Y. K. Vijay, *Int. J. Hydrogen Energy* **2011**, *36*, 6343–6355.
- [52] A. L. Kukla, Y. M. Shirshov, S. A. Piletsky, *Sens. Actuators B* **1996**, *37*, 135–140.
- [53] A. Hadi Ismail, Y. Sulaiman, *Synth. Met.* **2021**, *280*, 116860.
- [54] J. Li, L. Zhu, Y. Wu, Y. Harima, A. Zhang, H. Tang, *Polymer* **2006**, *47*, 7361–7367.
- [55] S. Pawar, M. Chougule, S. Patil, B. Raut, D. Dalvi, P. Patil, S. Sen, P. Joshi, V. Patil, *J. Sens. Technol.* **2011**, *1*, 16.
- [56] Y. D. Jo, S. Lee, J. Seo, S. Lee, D. Ann, H. Lee, *J. Nanosci. Nanotechnol.* **2014**, *14*, 9148–9151.
- [57] N. G. Deshpande, Y. G. Gudage, R. Sharma, J. C. Vyas, J. B. Kim, Y. P. Lee, *Sens. Actuators B* **2009**, *138*, 76–84.
- [58] Y. Seekaew, W. Pon-On, C. Wongchoosuk, *ACS Omega* **2019**, *4(16)*, 16916–16924.
- [59] S. G. Pawar, M. A. Chougule, S. L. Patil, B. T. Raut, P. R. Godse, S. Sen, V. B. Patil, *IEEE Sens. J.* **2011**, *11(12)*, 3417–3423.

Manuscript received: April 3, 2021
 Revised manuscript received: June 15, 2022
 Accepted manuscript online: June 17, 2022
 Version of record online: ■■■, ■■■■

RESEARCH ARTICLE

Ammonia is considered a hazardous air pollutant to human health and the environment. Here we developed hybrid platforms based on TiO₂ hollow nanofibers (obtained by coaxial electrospinning combined to calcination) and polyaniline for the monitoring of low concentrations of this pollutant. The obtained sensing platform showed fast response and high sensitivity towards ammonia detection at room temperature.



*P. P. Conti, Dr. D. M. dos Santos,
Dr. I. A. Goldthorpe, Dr. D. S. Correa**

1 – 9

**TiO₂ Hollow Nanofiber/Polyaniline
Nanocomposites for Ammonia
Detection at Room Temperature**